Journal of
Materials Chemistry A

Accepted Manuscript

This article can be cited before page numbers have been issued, to do this please use: S. Ramaprabhu and P. Divya, *J. Mater. Chem. A*, 2013, DOI: 10.1039/C3TA13070C.

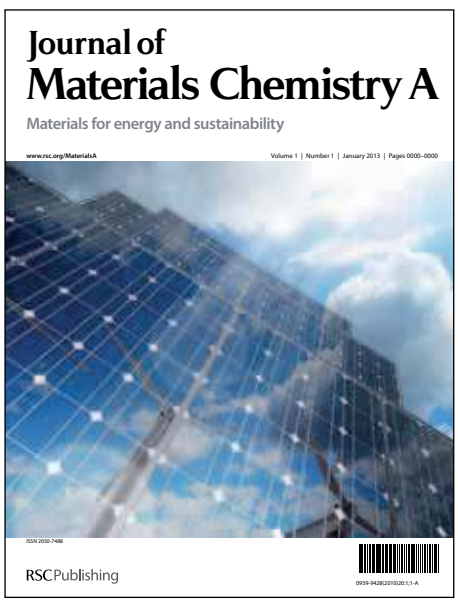

Journal of Materials Chemistry A

Dynamic Article Links ►
View Article Online
DOI: 10.1039/C3TA13070C

Cite this: DOI: 10.1039/c0xx00000x

www.rsc.org/xxxxxx

ARTICLE TYPE

Platinum nanoparticles supported on bi-metal oxide grown carbon nanostructure as ethanol electro-oxidation electrocatalyst

Divya P. and Ramaprabhu S.

Received (in XXX, XXX) Xth XXXXXXXXX 20XX, Accepted Xth XXXXXXXXX 20XX
DOI: 10.1039/b000000x

Development of inexpensive and highly active ethanol electro-oxidation electrocatalysts are a great challenge. Here, we report a novel material consisting of platinum dispersed on bi-metal oxide grown carbon nanostructure as ethanol electro-oxidation electrocatalyst. Carbon nanostructure has been synthesized by catalytic chemical vapour deposition of acetylene precursor over Fe-Sn-O particles. Platinum (Pt) nanoparticles have been decorated on bi-metal oxide grown carbon nanostructure (CNS-FSO) by polyol reduction technique. Suitability of the electrocatalyst for ethanol electro-oxidation is examined by cyclic voltammetry and amperometry techniques. Pt supported on CNS-FSO exhibited a higher catalytic activity towards ethanol electro-oxidation, in comparison to commercially available platinum on Vulcan XC-72 and platinum nanoparticles decorated functionalized multi walled carbon nanotube. This superior activity can be attributed to the unique properties of CNS-FSO as well as the synergic effect between platinum and CNS-FSO.

1. Introduction

Direct Ethanol Fuel Cell (DEFC) has received great attention than Direct Methanol Fuel Cell (DMFC) due to the advantages of fuel ethanol such as lower toxicity, exceptionally high theoretical mass energy density (8 vs. 6.1 kWh/Kg) and lower permeability across proton exchange membranes as compared to methanol[1, 2]. Moreover, easy and large scale production of ethanol from bio-mass and sugar containing raw materials are well established and this material is considered to be carbon neutral. As a liquid fuel, it avoids the risk of storage and transportation as compared to hydrogen based systems[3-5]. Despite these advantages, lack of an electrocatalyst that can efficiently deliver 12 electrons per ethanol molecule with carbon dioxide and water as by products is the major hurdle in the commercialization of DEFC[5, 6].

Ethanol electro-oxidation is complicated due to cleavage of c-c bond and by production of poisonous intermediates such as COads [7, 8]. Platinum is a well known electrocatalyst material for ethanol electro-oxidation. Even though platinum is considered as the best electrocatalyst material, oxidation of ethanol on platinum is limited up to acetaldehyde[9]. In addition, platinum is easily poisoned by CO like intermediates produced during dissociative adsorption of ethanol on platinum sites[3]. In this regard, it is necessary to develop more active and poison–resistant electrocatalysts that are superior to platinum. Tremendous efforts have been devoted to explore alternative electrocatalysts. Consequently, alloying Pt with less expensive transition metals such as Sn, Ir, Ru, Mo enhances ethanol electro-oxidation by oxidative removal of CO like intermediates[1, 2, 10-13]. Furthermore, it is reported that metal oxides which are present in the vicinity of Pt nanoparticles provide hydroxyl species (-OH) for the conversion of CO to CO_2. Already applied metal oxides in this context are MgO, SnO_2, TiO_2, CeO_2, $Ce_xZr_{1-x}O_2$[14-19] etc.

On the other hand, an ideal electrocatalyst support is necessary for the efficient utilization of an electrocatalyst. Carbon black is the most commonly used electrocatalyst support for fuel cell. The problem with carbon black is electrochemical corrosion which leads to the detachment of Pt nanoprticles hence electrochemical surface area get decreased[20, 21]. Intense research efforts have been devoted to the development of alternative electrocatalyst supports. Carbon nanotubes and carbon nanofibres have been widely applied as the electrocatalyst support for fuel cell because of their unique properties such as high electrical conductivity, surface area, and electrochemical corrosion resistance[14-16, 20, 22-24].

In the present investigation, we introduce platinum nanoparticles decorated on bi-metal oxide grown novel carbon nanostructure (Pt/CNS-FSO) as an electrocatalyst for ethanol electro-oxidation reaction. Carbon nanostructure (CNS) has been synthesized by catalytic chemical vapor deposition (CCVD) of acetylene gas over bi-metal oxide (Fe-Sn-O). Polyol reduction technique has been applied for platinum (Pt) nanoparticles decoration. The structural and morphological characterizations have been carried out by X-ray Diffraction (XRD), High Resolution Transmission Electron Microscope (HRTEM) and Field Emission Scanning Electron Microscope (FESEM), Fourier Transformed Infra Red spectroscopy (FTIR) and Raman Spectroscopy. Electrocatalytic activity of electrocatalysts for ethanol electro-oxidation is evaluated through cyclic voltammetry and amperometry techniques.

2. Experimental section

2.1 Materials

View Article Online
DOI: 10.1039/C3TA13070C

Ferric chloride ($FeCl_3$), tin chloride ($SnCl_2$), citric acid monohydrate ($C_6H_8O_7.H_2O$), ethylene glycol and ethanol used were analytical grade. Hexachloroplatinic acid (H_2PtCl_6 $6H_2O$) was supplied by Alfa Aesar. Deionized (DI) water was used for all the experiments. 20 percent platinum on Vulcan XC-72 (Pt/C) used was commercial.

2.2 Material synthesis

Carbon nanostructure was prepared by the catalytic chemical vapour deposition of acetylene precursor over the bi-metal oxide (Fe-Sn-O) catalyst. The as grown sample under gone air oxidation at 400 °C to remove amorphous carbon deposited on surface during the process. The final sample contains Fe-Sn-O along with CNS was named as CNS-FSO. Loading of Fe-Sn-O in the final sample is 17 wt% [25, 26]. Details of synthesis are provided in our previous paper as well as in †ESI.

Multi walled carbon nanotube (MWNT) were synthesized by catalytic chemical vapour deposition of carbon precursor, acetylene at 700 °C over AB_3 (A= misch metal, B=Ni) alloy hydride catalyst[27]. Detailed experimental procedure is given in †ESI. As grown MWNT undergone air oxidation at 400 °C to remove the amorphous carbon deposited during the growth process followed by refluxing the sample in concentrated nitric acid for 24 h at 60 °C removes the catalyst impurities. Then the sample was washed till neutral pH and dried in vaccum oven at 60 °C. Further, the MWNT were functionalized by ultrasonicating the sample in concentrated nitric acid for 3 h. Thereafter, the sample was washed till neutral pH, dried at 60 °C and labelled as f-MWNT.

Polyol reduction technique was followed for the dispersion of platinum nanoparticles over CNS-FSO/f-MWNT. Ethylene glycol acted as the reducing agent and hexachloroplatinic acid hexahydrate ($H_2PtCl_6.6H_2O$) was used as the platinum precursor. A suspension was made by ultrasonicating CNS-FSO/f-MWNT and $H_2PtCl_6.6H_2O$ in ethylene glycol. The suspension was stirred for 12 hours, refluxed at 130 °C around 4 hours and then cooled down to room temperature. Finally it was washed by distilled water and dried at 60 °C in vacuum oven. The loading of platinum maintained was 20 wt%. The Pt nanoparticles decorated CNS-FSO labelled as Pt/CNS-FSO[26] and Pt nanoparticles decorated f-MWNT labelled as Pt/f-MWNT.

2.3 Physical characterizations

Morphological analyses of the samples were carried out by a Quanta 3D field emission electron microscope (FESEM) and sample composition by elemental dispersive X-ray analysis (EDX). Tecnai F20 transmission electron microscope operated at 200 kV was used for high resolution transmission electron microscopy (TEM) imaging. Structural analysis was carried out by recording X-ray diffraction (XRD) patterns with a PANalytical X'Pert X-ray powder diffractometer, which operates with a CuKα1 radiation source of wavelength, λ=0.15406 nm. BET surface area was measured using BET analyzer (Micromeritics ASAP 2020). Identification of functional groups were carried out using PerkinElmer FT-IR spectrometer in the range 500–4000 cm-1. Raman analysis was done using a Confocal Raman spectrometer (WITec alpha 300) with an excitation source of Nd:YAG laser (532 nm).

2.4 Electrochemical measurements

The electrochemical experiments were conducted with a CHI 6083 electrochemical analyzer (CH instruments). A three electrode system was used for the measurement. Pt wire was used as the counter electrode and Ag/AgCl electrode saturated with 1M KCl was used as the reference electrode. The working electrode was fabricated as follows. Electrocatalyst ink was prepared by ultrasonicating electrocatalyst in ethanol and nafion solution (5 wt%). Amount of ethanol, electrocatalyst and Nafion used for electrocatalyst ink preparation were 100µl, 2mg and 5µl. A thin film of electrocatalyst was made by drop casting 2µl of the electrocatalyst ink onto a glassy carbon electrode (3mm in diameter) using micro pipette and the electrode kept till the electrocatalyst ink gets dried. In this study, the electrode potential was reported with respect to the Ag/AgCl electrode. The electrolyte used was 1M ethanol in 1M H_2SO_4. The electrocatalytic properties were investigated by recording cyclic voltammetry, and chronoamperometric curve.

3. Results and discussions

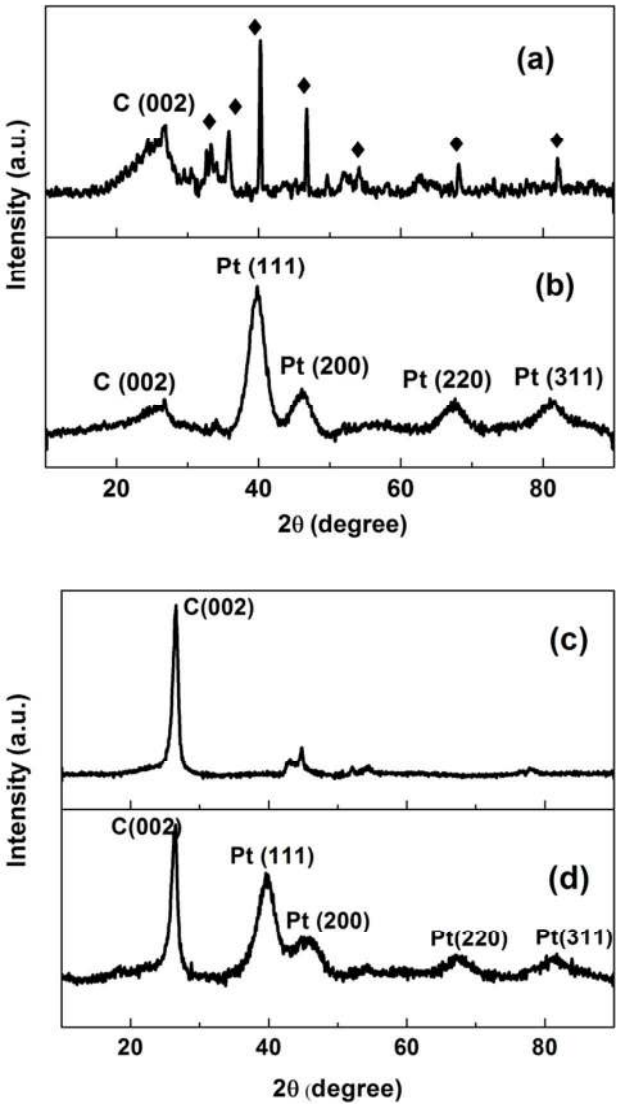

Figure 1. XRD of (a) CNS-FSO, (b) Pt/CNS-FSO, (c) MWNT and (d) Pt/f-MWNT

View Article Online
DOI: 10.1039/C3TA13070C

3.1 Structural and Morphological analysis

The physical characterizations of the sample are carried out by various characterization techniques. Figures 1 (a - d) show the XRD of the bi-metal oxide grown carbon nanostructure, Pt nanoparticles decorated on bi-metal oxide grown carbon nanostructures, MWNT and Pt decorated f-MWNT. In Figures 1(a & c), the diffraction peak at (002) plane corresponds to graphitic crystal structure. Other peaks in Figure 1(a) are assumed to be the peak positions of Fe-Sn-O. No alloy hydride peaks are observed in the XRD pattern of MWNT, since acid treatment removed all the catalyst impurities. In Figures 1 (b & d), the strong diffraction peaks are corresponding to Pt (1 1 1), Pt (2 0 0), Pt (2 2 0) and Pt (3 1 1) planes respectively. The peaks of bi-metal oxide are not visible in Figure 1(b), since it is hiding by the intense peaks of platinum. XRD of Pt/C (Figure S1) is given in †ESI.

The morphological characterizations and elemental analysis of the samples are carried out by SEM, TEM and EDX. SEM image, TEM image and EDX spectrum of Pt/C is given in †ESI. Figures 2 (a-h) show the SEM images and EDX patterns of CNS-FSO,

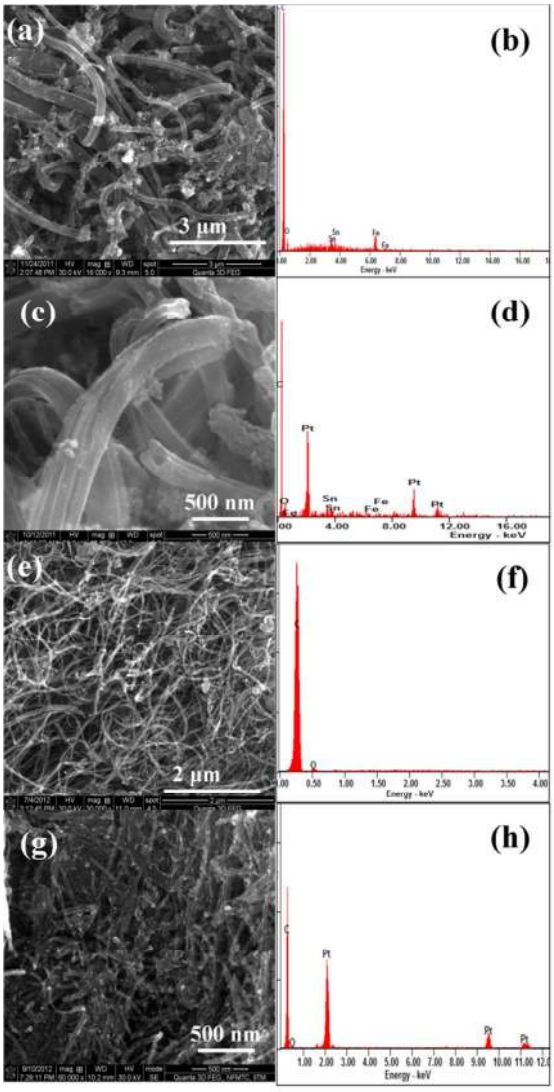

Figure 2. SEM images and EDX spectrum of (a & b) CNS-FSO, (c & d) Pt/CNS-FSO (e & f) MWNT and (g & h) Pt/f-MWNT

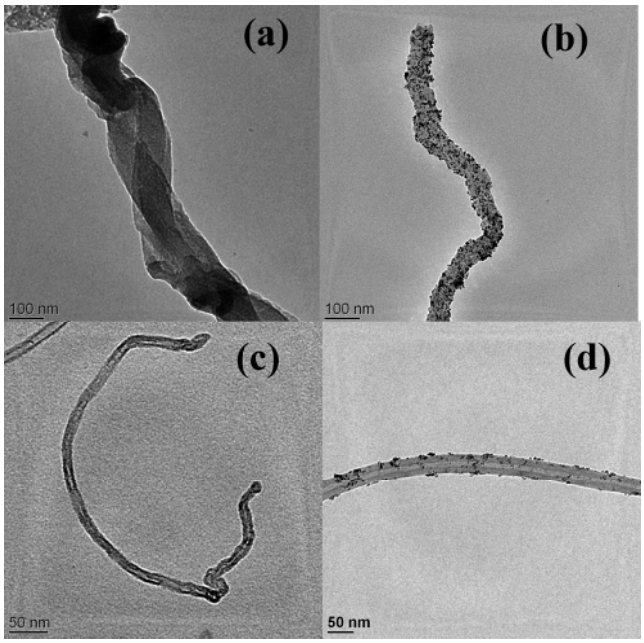

Figure 3. TEM images of (a) CNS-FSO (b) Pt/CNS-FSO,(c)MWNT and (d)Pt/f-MWNT

Pt/CNS-FSO, MWNT and Pt/f-MWNT. SEM images show the helical morphology of the CNS, tubular morphology MWNT as well as uniform distribution of Pt nanoparticles on CNS-FSO and f-MWNT. EDX spectrum of CNS-FSO (Figure 2(b)) shows the presence of C, O, Sn, and Fe in the sample and that of MWNT Figure 2(f) proves that catalyst impurities are completely removed by acid treatment. EDX spectrum Pt/CNS-FSO (Figure 2 (d)) shows the presence of Pt, Fe, Sn, O and C and that of Pt/f-MWNT (Figure 2(h)) shows the presence of Pt, O and C. The presence of Fe, Sn, O in CNS-FSO and Pt/CNS-FSO is due to the catalyst impurities remaining.

Figures 3 (a-d) show the TEM images of CNS-FSO and MWNT, Pt/CNS-FSO and Pt/f-MWNT. TEM images are shown in Figures 3(a & C) again confirm the helical structure of CNS-FSO and coaxial structure of MWNT respectively. Figures 3(b & d) reveal the suitability of ethylene glycol reduction method for

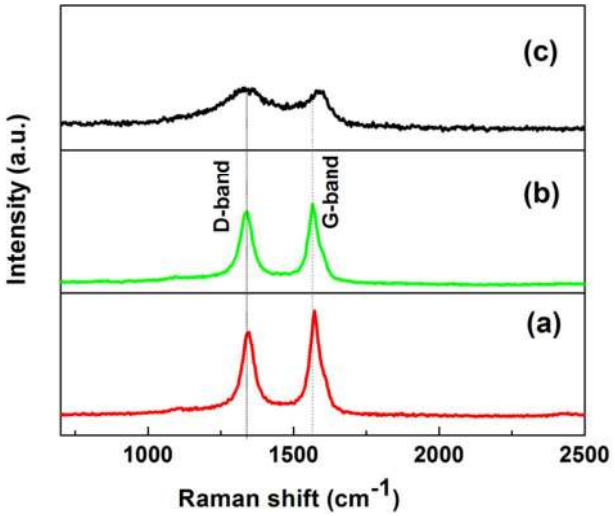

Figure 4: Raman spectra of (a) MWNT, (b) f-MWNT and (c) CNS-FSO.

View Article Online
DOI: 10.1039/C3TA13070C

uniform dispersion of fine platinum nanoparticles over CNS-FSO and f-MWNT. The mean particle size obtained from TEM is around 3-4 nm.

Figures 5 (a-c) show the Raman spectra of MWNT, f-MWNT and CNS-FSO respectively. The G-band is due to the Raman-active E_{2g} mode analogous to that of graphite, while D band is due to the defects or disorder present in MWNT and CNS-FSO[28-30]. The intensity of D-band is an indication of degree of disorder present. In f-MWNT, the intensity of the D-band is higher as compared to MWNT, since the acid functionalization introduces carboxyl and hydroxyl functional groups on MWNT which acts as anchoring sites for metal/metal oxide nanoparticles decoration[31]. In the case of CNS-FSO (Figure 5(c)), the intensity of D-band is higher than or comparable to that of G-band. This can be attributed to the presence of catalyst impurities (Fe-Sn-O) present in CNS-FSO. Furthermore, flat or helical structure also leads to increase the D-band intensity since these are the defective modification of tubular structure.

Presence of functional groups give hydrophilic nature to the material and these functional groups can act as anchoring sites for metal/ metal oxide nanoparticles decoration. FTIR is a tool normally used to identify the presence of functional groups such as hydroxyl, epoxy, carbonyl and carboxyl. Figure 6 (a-c) shows the FTIR spectrum of MWNT, f-MWNT and CNS-FSO respectively. Increase in the peak intensities of functional groups are observed in the case of f- MWNT and CNS-FSO (Figure 6 (b & c)), in comparison to MWNT (Figure 6(a)). The broad peak at 3450 cm^{-1} can be attributed to the stretching mode of -OH functional group present in the sample[32]. The peaks at 2924 cm^{-1} and 2873 cm-1 are attributed to the asymmetric (aCH_2) and symmetric (sCH_2) stretching vibrations of $–CH_2$. The peak at 1740 cm^{-1} is due to C=O, 1628 cm^{-1} is due to the C=C stretching mode and the peak at 1384 cm^{-1} is due C-O stretching vibrations of COOH groups[31, 33].

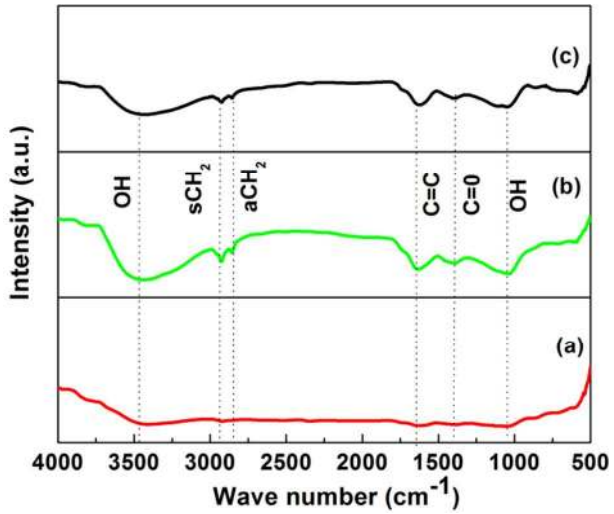

Figure 5: FTIR spectra of (a) MWNT, (b) f-MWNT and (c) CNS-FSO

3.2 BET surface area measurement

The Nitrogen adsorption and desorption isotherm for the CNS-FSO and MWNT is recorded using a BET analyzer is shown in Figure 6 (a & b). The BET surface area calculated is found to be

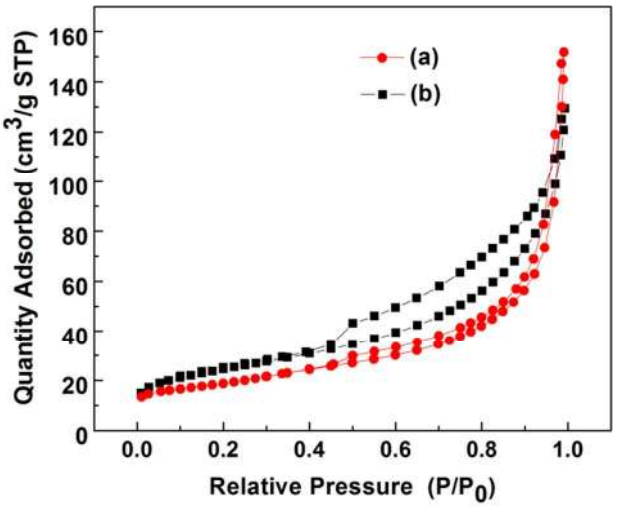

Figure 6. Nitrogen adsorption-desorption isotherm of (a) MWNT and (b) CNS-FSO

is high for CNS-FSO (85 m^2/g) in comparison to BET surface area of MWNT, which is 65 m^2/g. BET surface area reported for Vulcan XC-72 is 250 m^2/g [34-36]

3.3 Electrochemical studies

3.3.1 Cyclic voltammetry

The suitability of the electrocatalysts for ethanol electro-oxidation is first investigated by recording the cyclic voltammogram. The reverse scan oxidation peak in cyclic voltammogram (CV) can be attributed to the amount of poisoning intermediates formed during ethanol electro-oxidation. Generally, the ratio of forward anodic peak current density (I_f) to the reverse anodic peak current density (I_b) obtained from the cyclic voltammetry curve is used for investigating the tolerance of the electrocatalyst to the deposition of carbonaceous species. A low I_f/Ib ratio shows poor oxidation of alcohol to carbon dioxide during the anodic scan and excessive accumulation of unneeded intermediate species (carbonaceous residues) on the electrocatalyst surface. Hence the anti-poisoning ability can be investigated in terms of the ratio of forward peak current to reverse peak current[37-39]. Figures 4 (a-c) show the cyclic voltammogram of Pt/C, Pt/f-MWNT and Pt/CNS-FSO recorded at a scan rate of 50 mV/s in an electrolyte, which contains 1M ethanol in 1M H_2SO_4. The current has been normalized with area of the glassy carbon electrode which is called as current density and with loading of platinum which is reported as mass current. Ethanol oxidation current of Pt/CNS-FSO is 1.05 times high in comparison to that of Pt/f-MWNT. Ethanol oxidation current of Pt/C is 6.5 times less in comparison to Pt/CNS-FSO and 5.9 times less in comparison to that of Pt/f-MWNT. High ethanol electro-oxidation activity is observed in the case of Pt/CNS-FSO and Pt/f-MWNT as compared Pt/C. Though. CNS-FSO and MWNT shows low BET surface area as compared to Vulcan XC-72, high electrical conductivity of CNS-FSO and MWNT made Pt/CNS-FSO and Pt/f-MWNT superior to Pt/C. Peak ethanol oxidation mass current obtained for Pt/CNS-FSO and Pt/f-MWNT are 421 mA mg^{-1}_{pt} and 461 mA mg^{-1}_{pt} respectively. Peak current density reported for Pt/SWNT with a Pt loading of 40 μg cm^{-2} is 14 mA

View Article Online
DOI: 10.1039/C3TA13070C

cm^{-2} [40]. Hence, the mass current for Pt/SWNT is 350 mA mg^{-1}_{pt}, which is low in comparison to that of Pt/CNS-FSO and Pt/f-MWNT. The CO poisoning tolerance evaluated in terms of the ratio of forward peak current to reverse peak current (I_f/I_b). I_f/I_b for Pt/C, Pt/f-MWNT and Pt/CNS-FSO are tabulated in Table1. High I_f/I_b ratio favours the higher ethanol electro-oxidation activity of Pt/CNS-FSO as compared to Pt/C and Pt/f-MWNT. I_f/I_b obtained for Pt/f-MWNT is low as compared to Pt-Sn/f-MWNT (1.55) [39]. It is reported that Sn and SnO_2 can provide oxygen containing species to the oxidation of CO adsorbed species on platinum sites.[41-44]. I_f/I_b ratio obtained for Pt/CNS-FSO is comparable to I_f/I_b (1.55), reported for Pt-Sn/f-MWNT. Here, bi-metal oxide may do the same function as Sn did in the case of ethanol oxidation. As a result, more active platinum sites can be free for ethanol electro-oxidation. On the other hand, a low cost bi metal oxide has been used for the synthesis of CNS-FSO made it a cost effective electrocatalyst support as compared to MWNT. Besides, acid treatment typically used to remove catalyst impurities has been avoided since it may introduce oxygen-containing functional groups which in turn reduce the electrical conductivity[45].

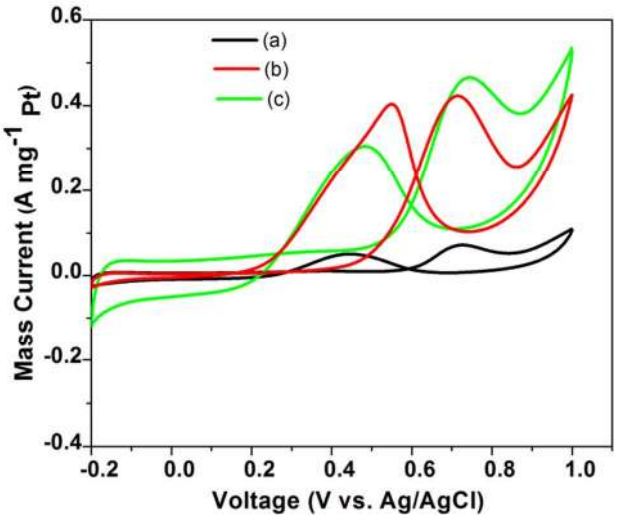

Figure 7. Cyclic voltammograms of (a) Pt/C (b) Pt/f-MWNT and (c) Pt/CNS-FSO in 1M H_2SO_4 and 1M C_2H_5OH

Table 1 I_f/I_b obtained for Pt/C, Pt/f-MWNT as well as Pt/CNS-FSO in 1M H_2SO_4 and 1M C_2H_5OH.

Material	Pt/C	Pt/f-MWNT	Pt/CNS-FSO
I_f/I_b [a]	1.421±0.013	1.045±0.016	1.527±0.021

a I_f/I_b is the ratio of forward peak current to the reverse peak current obtained from Figure 7

3.3.2 Amperometric measurements

The long term electrochemical stability and catalytic activity of Pt/C, Pt/f-MWNT and Pt/CNS-FSO for ethanol oxidation was investigated at room temperature by chronoamperometric experiment. Figure 6 (a-c) shows the amperometric curve (current-time profile) recorded for Pt/C, Pt/f-MWNT and Pt/CNS-FSO respectively. The electrolyte used was a solution of 1M ethanol in 1 M H_2SO_4. The applied potentional was 0.4 V with respect to Ag/AgCl reference electrode. The current drops with time and it will reach in stable state after some time. This can be attributed to the adsorption of incompletely oxidized intermediates during ethanol electrooxidation. Over the entire range shown in Figure 8, Pt/CNS-FSO has higher stability in comparison to Pt/C and Pt/f-MWNT. This can be attributed to the high CO poisoning tolerance of Pt/CNS-FSO. Though Pt/C shows high CO poisoning tolerance in comparison to Pt/f-MWNT, current decays fast. This can be attributed to the high corrosion resistance, unique crystallographic and electronic properties of graphitic carbon in comparison to amorphous carbon. Uniform distribution and strong adhesion of platinum nanoparticles on electrocatalyst support also has significant impact on the stability of the electrocatalyst.

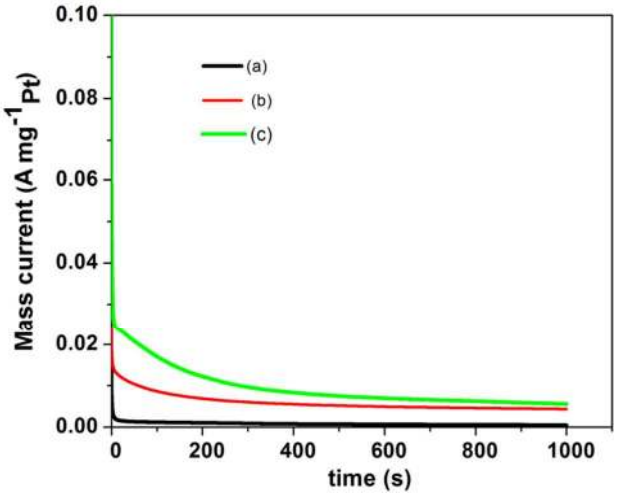

Figure 8. chronoamperometric curves of (a) Pt/C and (b) Pt/f-MWNT and (c) Pt/CNS-FSO in 1M H_2SO_4 and 1M C_2H_5OH

Conclusions

In summary, the electrocatalyst support material (CNS-FSO) has been synthesized by CCVD method and Pt nanoparticles decorated by ethylene glycol reduction through which uniform dispersion of Pt nanoparticles over the surface has been achieved. The electrochemical studies show the superior ethanol electro-oxidation activity as well as anti poisoning capacity of Pt/CNS-FSO, in comparison to Pt/f-MWNT and state-of-the-art electrocatalyst, Pt/C. This can be attributed to the uniform dispersion of ultrafine platinum nanoparticles over the electrocatalyst support by ethylene glycol reduction method, defective structure and higher electrical conductivity of carbon nanostructures. In addition to that, the presence of bi-metal oxide favours the removal of poisonous intermediates such as CO produced during ethanol electro-oxidation. Hence, Pt/CNS-FSO can be considered as a promising ethanol electro-oxidation electrocatalyst.

Acknowledgement

The authors wish to thank Indian Institute of technology Madras for supporting this work and SAIF, IIT Madras for FTIR characterization. One of the authors is thankful to Council of Scientific and Industrial Research (CSIR), India for SRF assistance.

View Article Online
DOI: 10.1039/C3TA13070C

Notes and references

*Alternative Energy and Nanotechnology Laboratory (AENL), Nano Functional Materials Technology Centre (NFMTC), Department of Physics, Indian Institute of Technology Madras, India. * Phone: +91-44-22574862; E-mail: ramp@iitm.ac.*

† Electronic Supplementary Information (ESI) available: [XRD, SEM, EDX and TEM analysis of Pt/C.Cyclic voltammogram of Pt/C, Pt/f-MWNT and Pt/CNS-FSO]. See DOI: 10.1039/b000000x/

1. J. Tayal, B. Rawat and S. Basu, *International Journal of Hydrogen Energy*, 2011, **36**, 14884-14897.
2. N. Fujiwara, K. A. Friedrich and U. Stimming, *Journal of Electroanalytical Chemistry*, 1999, **472**, 120-125.
3. C. Lamy, E. M. Belgsir and J. M. Léger, *Journal of Applied Electrochemistry*, 2001, **31**, 799-809.
4. C. C. A. Y.Ye, C. Witham, B. Fultz, J. Liu, A. G. Rinzler, D. Colbert, K. A. Smith, and R. E. Smalley, *Applied Physics Letters*, 1999, **74**, 1999-2001.
5. J. Mann, N. Yao and A. B. Bocarsly, *Langmuir*, 2006, **22**, 10432-10436.
6. J. Ribeiro, D. M. dos Anjos, K. B. Kokoh, C. Coutanceau, J. M. Léger, P. Olivi, A. R. de Andrade and G. Tremiliosi-Filho, *Electrochimica Acta*, 2007, **52**, 6997-7006.
7. F. Vigier, C. Coutanceau, A. Perrard, E. M. Belgsir and C. Lamy, *Journal of Applied Electrochemistry*, 2004, **34**, 439-446.
8. M. Sawangphruk, A. Krittayavathananon and N. Chinwipas, *Journal of Materials Chemistry A*, 2013, **1**, 1030-1034.
9. D. J. Tarnowski and C. Korzeniewski, *The Journal of Physical Chemistry B*, 1997, **101**, 253-258.
10. Z. Liu, X. Y. Ling, X. Su, J. Y. Lee and L. M. Gan, *Journal of Power Sources*, 2005, **149**, 1-7.
11. H. Herrera-Méndez, P. Roquero, M. Smit and L. Ordóñez, *Int. J. Electrochem. Sci*, 2011, **6**, 4454-4469.
12. W. Zhou, S. Song, W. Li, G. Sun, Q. Xin, S. Kontou, K. Poulianitis and P. Tsiakaras, *Solid State Ionics*, 2004, **175**, 797-803.
13. W. Du, Q. Wang, C. A. LaScala, L. Zhang, D. Su, A. I. Frenkel, V. K. Mathur and X. Teng, *Journal of Materials Chemistry*, 2011, **21**, 8887-8892.
14. B. Liu, J. Chen, C. Xiao, K. Cui, L. Yang, H. Pang and Y. Kuang, *Energy & fuels*, 2007, **21**, 1365-1369.
15. X. Zhang, H. Zhu, Z. Guo, Y. Wei and F. Wang, *Journal of Power Sources*, 2011, **196**, 3048-3053.
16. H. Song, X. Qiu, F. Li, W. Zhu and L. Chen, *Electrochemistry communications*, 2007, **9**, 1416-1421.
17. H. Song, X. Qiu, X. Li, F. Li, W. Zhu and L. Chen, *Journal of power sources*, 2007, **170**, 50-54.
18. C. Xu and P. K. Shen, *Journal of power sources*, 2005, **142**, 27-29.
19. Y. Bai, J. Wu, X. Qiu, J. Xi, J. Wang, J. Li, W. Zhu and L. Chen, *Applied Catalysis B: Environmental*, 2007, **73**, 144-149.
20. A. L. Dicks, *Journal of Power Sources*, 2006, **156**, 128-141.
21. Y. Shao, J. Wang, R. Kou, M. Engelhard, J. Liu, Y. Wang and Y. Lin, *Electrochimica Acta*, 2009, **54**, 3109-3114.
22. J. Jung, B. Park and J. Kim, *Nanoscale research letters*, 2012, **7**, 1-8.
23. A. Tabet-Aoul and M. Mohamedi, *Journal of Materials Chemistry*, 2012, **22**, 2491-2497.
24. F. Alcaide, G. Álvarez, O. Miguel, M. J. Lázaro, R. Moliner, A. López-Cudero, J. Solla-Gullón, E. Herrero and A. Aldaz, *Electrochemistry Communications*, 2009, **11**, 1081-1084.
25. D. Li, L. Pan, J. Qian and D. Liu, *Carbon*, 2010, **48**, 170-175.
26. D. Puthusseri, T. T. Baby, V. Bhagavathi Parambhath, R. Natarajan and R. Sundara, *International Journal of Hydrogen Energy*, 2013.
27. A. L. M. Reddy, M. Shaijumon and S. Ramaprabhu, *Nanotechnology*, 2006, **17**, 5299.
28. A. C. Ferrari and J. Robertson, *Physical Review B*, 2000, **61**, 14095-14107.
29. M. S. Dresselhaus, A. Jorio, M. Hofmann, G. Dresselhaus and R. Saito, *Nano Letters*, 2010, **10**, 751-758.
30. W. Qian, T. Liu, F. Wei, Z. Wang, G. Luo, H. Yu and Z. Li, *Carbon*, 2003, **41**, 2613-2617.
31. A. K. Mishra and S. Ramaprabhu, *The Journal of Physical Chemistry C*, 2010, **114**, 2583-2590.
32. Z. L. X. Sun, K. Welsher, J. T. Robinson, A. Goodwin, S. Zaric and H. Dai, *Nano Research*, 2008, **1**, 203.
33. U. J. Kim, C. A. Furtado, X. Liu, G. Chen and P. C. Eklund, *Journal of the American Chemical Society*, 2005, **127**, 15437-15445.
34. L. R. Jordan, A. K. Shukla, T. Behrsing, N. R. Avery, B. C. Muddle and M. Forsyth, *Journal of Applied Electrochemistry*, 2000, **30**, 641-646.
35. J. Prabhuram, T. S. Zhao, C. W. Wong and J. W. Guo, *Journal of Power Sources*, 2004, **134**, 1-6.
36. M. Williams, L. Khotseng, Q. Naidoo, L. Petrik, A. Nechaev and V. Linkov, *South African Journal of Science* 2009, **105**, 285-289.
37. M. Hasan, S. B. Newcomb, J. F. Rohan and K. M. Razeeb, *Journal of Power Sources*, 2012.
38. Z. Liang, T. Zhao, J. Xu and L. Zhu, *Electrochimica Acta*, 2009, **54**, 2203-2208.
39. R. I. Jafri and S. Ramaprabhu, *International Journal of Hydrogen Energy*, 2010, **35**, 1339-1346.
40. R. S. Hsu, D. Higgins and Z. Chen, *Nanotechnology*, 2010, **21**, 165705-116509.
41. L. Jiang, L. Colmenares, Z. Jusys, G. Q. Sun and R. J. Behm, *Electrochimica Acta*, 2007, **53**, 377-389.
42. A. Kowal, S. L. Gojković, K. S. Lee, P. Olszewski and Y. E. Sung, *Electrochemistry Communications*, 2009, **11**, 724-727.
43. L. Jiang, Z. Zhou, W. Li, W. Zhou, S. Song, H. Li, G. Sun and Q. Xin, *Energy & Fuels*, 2004, **18**, 866-871.
44. H. Li, G. Sun, L. Cao, L. Jiang and Q. Xin, *Electrochimica Acta*, 2007, **52**, 6622-6629.
45. C. Lau, R. Cervini, S. Clarke, M. Markovic, J. Matisons, S. Hawkins, C. Huynh and G. Simon, *J Nanopart Res*, 2008, **10**, 77-88.